POLITECNICO
MILANO 1863

SCUOLA DI INGEGNERIA INDUSTRIALE
E DELL'INFORMAZIONE

Executive Summary of the Thesis

Design and deployment of a dual-illumination automated system for epifluorescence imaging in cultural heritage

Laurea Magistrale in Engineering Physics - Ingegneria Fisica

Author: Gaia Sperandio

Advisor: Prof.ssa Daniela Comelli

Co-advisor: Dott. Francesco Carta

Academic year: 2025-2026

---

1. Introduction to photoluminescence

Photoluminescence is the emission of light due to radiative de-excitation by materials following optical excitation, and it is a valuable probe of their physical and chemical properties.
Depending on the nature of the excited state, photoluminescence is classified into fluorescence and phosphorescence: fluorescence originates from spin-allowed transitions and is characterized by decay times ranging from hundreds of picoseconds to hundreds of nanoseconds; phosphorescence, on the other hand, involves spin-forbidden transitions through excited triplet states, and thus exhibits way longer lifetimes, from microseconds to even minutes [1].
The study of photoluminescence has become an important tool in cultural heritage diagnostics, because it allows the investigation of artworks through minimally invasive or completely non-invasive techniques. Imaging techniques based on photoluminescence (from UV-induced photography to hyperspectral and lifetime imaging) provide information on the luminescent materials present on the surface of a work of art. When dealing a painting, these can include varnishes, binding media, restoration materials, colourants and luminescent pigments [2, 3]; a specific class of luminescent pigments include semiconductor and inorganic crystalline pigments, where photoluminescence can originate from intrinsic radiative recombination across the bandgap, but also from localized defects and trap states within the energy gap [4]. The first one typically results in radiative lifetimes in the nanosecond range, while defect-related luminescence can persist for microseconds or milliseconds: these markedly different temporal behaviours can contribute to distinguishing materials, especially with similar spectral responses.
Conventional UV-induced fluorescence photography offers qualitative information; on the other, time-resolved techniques exploit the temporal evolution of the emitted signal to improve material discrimination, which is particularly valuable for inorganic pigments – distinguished from organic materials such as varnishes and binding media due to their longer decay times.
This thesis falls within this context; specifically, it aims to design a novel microscopy setup capable of combining conventional fluorescence imaging with photoluminescence lifetime imaging, as detailed in the next section.

2. Microscopy techniques

Optical microscopy forms magnified images of microscopic specimens through objectives, illumination optics and detectors. In particular, in epifluorescence microscopy, excitation and emitted fluorescence share the same objective, while an excitation filter, a dichroic mirror and an emission filter, whose spectral characteristics match the luminescent properties of the sample, selectively direct the excitation light and isolate the fluorescence emission.
The experimental work presented in this thesis is based on a Leica DM RE epifluorescence microscope, whose incident-light optical path already incorporates Kohler illumination of a halogen visible lamp (or an interchangeable mercury lamp) together with interchangeable fluorescence filter and reflector cubes. This existing microscope allows a rapid switch between sample observation under visible light and observation of the luminescent emission from the sample by selecting the appropriate illumination source and filter cube.
Conventional fluorescence microscopy provides spatial information on the distribution of luminescent materials; however, it does not exploit the decay kinetic of the emitted signal. Fluorescence Lifetime IMaging (FLIM) complements it, sampling the fluorescence decay after a pulsed excitation at every pixel of the image.

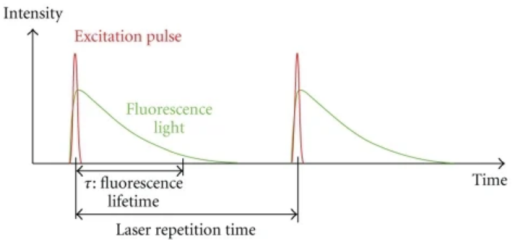

Figure 1: Pulsed laser excitation and photoluminescence response, in intensity over time.

The objective of this work is to extend the capabilities of the Leica DM RE microscope and integrate a laser excitation for epifluorescence microscopy and FLIM, while still preserving the lamp-illuminated microscopy.
Before describing in-depth the design of the innovative microscopy setup developed, a brief description of the FLIM setup employed is given. It consisted of a pulsed Nd:YAG laser operating at 355 and 532 nm for sample excitation, a time-gated intensified CCD (ICCD) camera for fluorescence detection, and a delay generator synchronized to the laser through a custom constant-fraction trigger unit. Through a fit with a mono-exponential decay model, three maps of the field of view are obtained: a fluorescence intensity map, a lifetime map in false colours, and an HSV map – which maps in each pixel the saturation value from the intensity of fluorescence, and the hue from the lifetime.

3. Design of the setup

Since the Leica DM RE microscope provides no native interface for laser coupling, the design challenge is to develop a solution that could be integrated into the instrument without modifying its architecture.

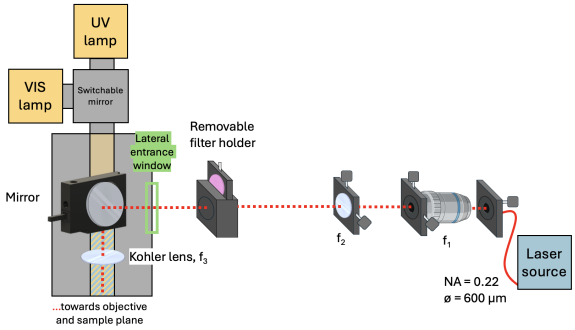

Figure 2: Top view scheme of the ILIF setup (in green) when integrated in the Leica microscope.

The proposed solution is named ILIF ("Ingresso Laterale In Fibra", Italian for "lateral fiber entrance") as it exploits a lateral access with a dovetail railing available on the microscope to inject the laser beam into the illumination path; an automated movable mirror reflects the beam by 90° when needed, to align it to the internal optical axis, while moving it out of the optical path during conventional visible or fluorescence microscopy, allowing the original lamp illumination to remain completely available and enabling rapid switching between the two illumination modes while maintaining both the eyepiece and camera detection paths unaltered.
The design process combined optical, mechanical and electronic development. A preliminary characterization of the microscope was first carried out to determine the available installation volume, identify the internal geometrical constraints for the insertion and experimentally

characterize the unknown optical parameters required for the design. The optical path of the Leica microscope shared with the ILIF system is a generalized 4f system comprised of a lens, called Kohler lens, whose focal length is experimentally measured to be 54 mm, and the refractive objective of the microscope (alternately a 10x or a 50x, both infinity-corrected) – as in Fig. 3. Detection happened from either the eyepieces or the tube lens (of focal length 250 mm, given by the manufacturer).

3.1. Optical simulations and design

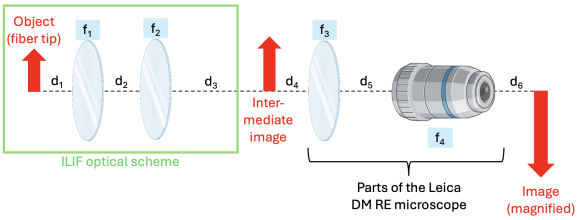

Figure 3: Scheme of the ILIF and the pre-existing Leica optical components.

The illumination optics was designed through a combination of analytical modelling and numerical simulations, while respecting two general requirements imposed: (i) a uniform illumination in the sample plane, achieved by creating an image of the excitation multimode fiber at the sample plane; (ii) a fiber image size $\gtrsim 80\%$ of the field of view's diameter – measured to be 1.8 mm with a 10x objective (and 360 μm with a 50x). Therefore, illuminating with a NA=0.22, 600 μm silica multimode fiber and considering the Leica optics, the ILIF should have a magnification factor of $M_{ILIF} \in [-6.48, -5.83]$.
To form this intermediate image that the generalized 4f system of the microscope could further magnify (as in Fig. 3), a two-lens configuration was chosen. First, through the mathematical software Maple a first-order estimate in matrix optics was obtained for the distances d_1 (fiber tip to first lens), d_2 (interlens) and d_3 (second lens to intermediate image), while varying the focal lengths of the two lenses. Then, ray-tracing simulations were done with Zemax to instead evaluate commercially available lens options, optimise their distances and predict the illumination spot performance for selected testing wavelengths (355 nm, 532 nm and 633 nm). The best results in terms of wanted magnification and aberrations of the system are obtained with these two lenses:

- UV Fused Silica Plano-Convex Lens LA4647, EFL $f_1 = 20.1$ mm, diameter 12.7 mm, for $\lambda \in 185$ nm - 2.1 μm;
- UV Fused Silica Plano-Convex Lens LA4380-A, EFL $f_2 = 100.3$ mm, diameter 25.4 mm, AR coated for $\lambda \in 350$-700 nm.

Finally, the chosen lenses were experimentally tested; in order to improve spherical and chromatic aberration correction, the first optical element was replaced in the experimental setup by a 10x microscope objective (Leitz Wetzlar PL Fluotar 10x, NA = 0.30, focal length ≈ 16 mm). Experimental testing confirmed the design: at 532 nm the intermediate image diameter was 3.55 mm (magnification of 5.92, in excellent agreement with the simulated value of 5.95 and within the design requirement). At 355 nm, the focus shifted by 2 mm because of longitudinal chromatic aberration and the image diameter decreased to 2.7 mm due to transverse chromatic aberration; still, these results validated the optical design before its integration into an assembly.

3.2. Mechanical design

The optical assembly was integrated into a custom-designed mechanical block to fit in the internal geometry of the Leica microscope. A mirror holder was custom-designed to fit a 1 inch dielectric mirror, actuated by a miniature stepper motor through the use of two 3D printed gears, allowing repeatable movements between the two configurations despite the limited space available inside the microscope housing. In addition, two pins were printed poking out of two sides of the mirror holder to signal to two optical endstops, communicating with a microcontroller and attached to the custom block through a 3D printed custom-designed base, what the maximum range of motion was.

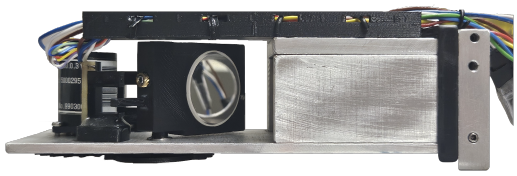

Figure 4: Final ILIF block; rightmost, the cage system adapter plate, in metal; on the left, the stepper motor, one of the two endstops, and the mirror holder.

3.3. Automation, coding and touchscreen

The automation of the system was implemented using an Arduino-based program; besides controlling the mirror positioning via absolute and relative movements, the software manages an initialization procedure, safety procedures when reaching the end of the range of motion, and user interaction through an appositely implemented touchscreen customized graphical interface, allowing the complete operation of the illumination system with user ease and without requiring a computer interface. The resulting platform provides an integrated solution in which the optical, mechanical and electronic subsystems operate together to extend the functionality of the microscope while preserving its original versatility.

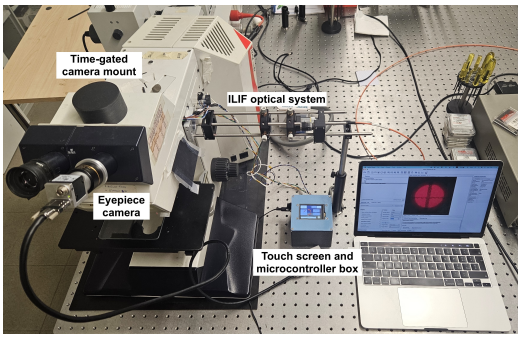

Figure 5: Fully functional ILIF setup in use for optical microscopy.

4. Validation of the setup

Following the design and its integration, the developed setup was experimentally validated to assess its optical performance, transmission efficiency and mechanical repeatability. First of all, however, a procedure was carried out to align the beam reflected by the mirror to the microscope's optical axis, by iteratively adjusting the two x-y translation stages supporting the ILIF lenses until the laser beam was coaxial with the internal optical axis, producing a well-defined image of the fiber on the sample plane without evidence of vignetting or beam clipping.

4.1. Spot sizes

The illumination spot generated on the sample plane was characterized using a calibrated microscope slide and a Q-switched Nd:YAG laser (FTSS 355-50, CryLaS GmbH, pulse FWHM = 1.0 ns, repetition rate = 100 Hz, average power = 7 mW, peak power = 50-80 kW) emitting at either 532 nm or 355 nm. With the 10x objective, the measured spot diameter was approximately 1.60 mm ± 0.1 mm at 532 nm and 1.5 mm ± 0.1 mm at 355 nm, corresponding to about 89% and 83% of the microscope field of view, respectively. The smaller UV spot is consistent with the transverse chromatic aberration predicted by the simulations, but still satisfies the design requirements.

4.2. Power transmission

The optical transmission of power by the system was evaluated by measuring the laser power at different locations along the optical path with a thermopile sensor; the results are displayed in Table 1.

λ	Fiber	ILIF	Sample
532 nm	4.0 mW	3.0 mW	1.3 mW
355 nm	2.7 mW	0.55 mW	0.23 mW

Table 1: Power after different parts of the setup.

While the visible measurements for the ILIF optics agree well with the theoretical estimates based on a 5% reduction at each optical surface due to Fresnel reflections, the lower ultraviolet transmission can be attributed to the reduced UV transmittance of the microscope objective used as the first optical element, which is not specifically designed for ultraviolet operation. Nevertheless, the absence of additional unexpected losses confirms that the optical relay was correctly designed and aligned.

4.3. Repeatability

The repeatability of the motorized mirror positioning was assessed by repeatedly switching the illumination system to and from the laser configuration, capturing a picture and analysing the position of the centroid of the laser spot. At 10x magnification, the standard deviations of the beam position were 19.3 μm along the horizontal motion direction and 5.77 μm along the vertical one, corresponding to an overall positioning uncertainty of approximately 1.1% of the field of view. A second characterization performed at 50x magnification confirmed the stability of the positioning system, yielding σ_x =

5.36 μm, $\sigma_y = 0.79\mu$m and an an overall uncertainty of $\simeq 1.5\%$ of the FOV at 50x. No measurable temporal drift was observed during the acquisitions, demonstrating the long-term stability of both the optical alignment and the automation setup.

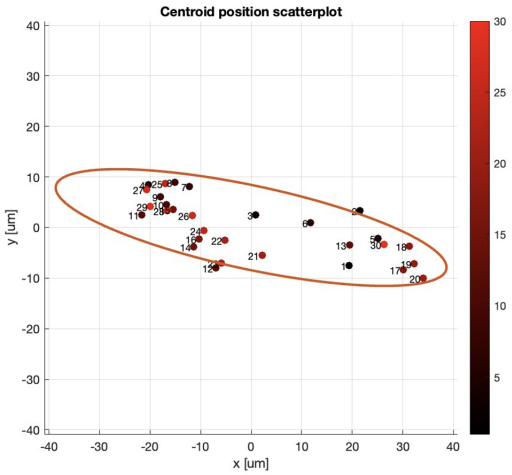

Figure 6: Scatterplot of the laser spot centroid positions, imaged with a 10x objective; the colorbar references the image number.

4.4. Gear backlash

The positioning accuracy of the motorized mirror is influenced by the mechanical backlash of the gears of the stepper motor and the mirror holder. Repeated forward and reverse movements while monitoring the beam spot position revealed a reproducible 22-step backlash. This value was implemented as a software compensation in the Arduino code, effectively eliminating the positioning error without mechanical modifications.

4.5. Image coregistration

Finally, the compatibility between the optical microscopy images (obtained with a colour eyepiece camera) and FLIM acquisitions was verified through image coregistration. An affine transformation matrix was estimated using the image processing package Fiji: the obtained transformation (made of a rototranslation and a scaling of the image), compensates for the geometric differences between the eyepiece camera and the ICCD detector, enabling accurate spatial correspondence between the images. In the particular case of Fig. 7, the resulting transformation features a translation of 84 pixels to the left and 272 pixels downward, together with a rotation of about 4.7^o and a small anisotropic scale adjustment: horizontally, the scaling factor is ≈ 0.9632 horizontally, while vertically it is ≈ 0.8069. Applying this transformation, the geometric discrepancies between the two acquisitions are compensated, and the complementary information provided by the two imaging modalities can be compared directly pixel-wise.

5. Analysis of Artistic Samples

The capabilities of the system were deployed in the analysis of artistic materials using visible light microscopy, UV-induced fluorescence microscopy and time-gated FLIM. Two case studies were investigated: a paint cross-section sampled from an untitled painting (c. 1912–1913) by Russian painter Mikhail Larionov and a powder sample of Chilean ultramarine blue pigment. For brevity, only the results obtained on the Larionov stratigraphy are presented here, as they provide a comprehensive example of the complementary information obtained through the different imaging modalities.
The investigated cross-section, embedded in epoxy resin, consists of three pictorial layers: the stratigraphic morphology revealed in dark-field optical microscopy distinguished a heterogeneous yellow upper layer, an underlying white layer containing localized brown inclusions, and a thin blue layer (Fig. 7c).

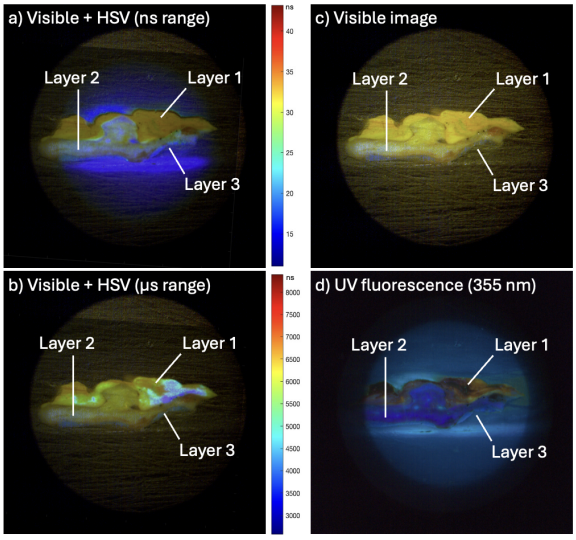

Figure 7: L5 sample at 10x objective magnification ("+" means coregistration).

Under pulsed 355 nm excitation, the stratig-

raphy exhibits a heterogeneous fluorescence response across its different layers. Layers 2 and 3 are dominated by an homogeneous bright blue emission, while the upper yellow paint layer displays localized yellow, orange and white luminescent regions, with noticeable spatial variations (Fig. 7d).
The time-resolved measurements provided additional contrast that could not be otherwise obtained from fluorescence intensity alone. Nanosecond-gated acquisitions revealed short-lived emissions from the second and third layers, with characteristic lifetimes of approximately 15 ns, whereas the upper yellow layer exhibited substantially longer decay components. Extending the acquisition to the microsecond timescale allowed to investigate these further: the upper layer displayed a highly heterogeneous nature, with the lowest, yellow-emitting stripe of layer 1 exhibiting shorter decay lifetimes than the upper yellow pigment, emitting a reddish-brown colour. The third layer also exhibited decay times of approximately 5 μs, shorter than the longer-lived emission observed in layer 2. The spatial coregistration between the FLIM maps and the visible images enabled these lifetime distributions to be directly associated with the corresponding pictorial features.
The measured luminescence behaviour is consistent with previous investigations of the same sample reported in the literature [5], where complementary spectroscopic techniques (such as time-resolved photoluminescence spectroscopy) identified cadmium yellow in layer 1, zinc white in layer 2 and synthetic ultramarine blue in layer 3 as the principal pigments. The agreement with previous spectroscopic studies confirms that the developed system provides reliable fluorescence lifetime maps and meaningful complementary information for the investigation of cultural heritage materials.

6. Conclusions and future developments

The developed system successfully adapts a commercial research microscope for conventional optical microscopy, epifluorescence microscopy and time-resolved imaging, preserving its original optical and geometrical architecture – which constituted the main challenge of the project. The combination of optical design, mechanical integration, electronics and software resulted in a compact and versatile module that was experimentally characterized in terms of illumination spot, optical transmission and mechanical repeatability. The system proved capable of rapidly switching between lamp illumination and pulsed laser excitation, but also of acquiring conventional optical images together with fluorescence intensity and lifetime maps on the same microscope, without repositioning the sample. Its application to a paint microstratigraphy from Mikhail Larionov's painting demonstrated that the setup allows the coregistration between FLIM maps and optical microscopy pictures, which improve interpretability of the data, with results in agreement with previous literature.
Several opportunities remain for further development, such as an improvement of the optical efficiency at ultraviolet wavelengths through the adoption of UV-optimized optical components. A particularly promising development would be the integration of Time-Gated Hyperspectral Imaging (TG-HSI) through the TWINS (Translating-Wedge-based Identical pulses eNcoding System) interferometer, which retrieves spectral information by generating two phase-locked replicas of the emitted light and measuring their interferogram, which, once Fourier-transformed, can reconstruct the spectrum.
By integrating the time-gated hyperspectral imaging module, it will be possible to obtain a highly spatially-resolved picture of the field of view, but also the fluorescence decay and the full photoluminescence spectrum for every pixel. This simultaneous availability of spatial, temporal and spectral information would significantly improve the identification possibilities for luminescent materials, thus providing a more comprehensive and multidimensional optical characterization of complex artistic samples and broadening its applicability to cultural heritage diagnostics.

References

[1] Joseph R. Lakowicz. *Principles of fluorescence spectroscopy*. Springer, third edition, 2010. ISBN 0387312781.

[2] Austin Nevin, Anna Cesaratto, Sara Bellei, Cosimo D'Andrea, Lucia Toniolo, Gianluca

Valentini, and Daniela Comelli. Time-resolved photoluminescence spectroscopy and imaging: New approaches to the analysis of cultural heritage and its degradation. *Sensors*, 14(4):6338–6355, 2014. doi: 10.3390/s140406338.

[3] Daniela Comelli, Gianluca Valentini, Rinaldo Cubeddu, Chiara Colombo, and Lucia Toniolo. Fluorescence lifetime imaging and spectroscopy as tools for nondestructive analysis of works of art. *Applied Optics*, 43 (10):2175–2183, 2004. doi: 10.1364/AO.43.002175.

[4] Audrius Alkauskas, Matthew D. McCluskey, and Chris G. Van De Walle. Defects in semiconductors - Combining experiment and theory. *Journal of Applied Physics*, 119(18), 2016. doi: 10.1063/1.4948245.

[5] Alessia Artesani, Marta Ghirardello, Sara Mosca, Austin Nevin, Gianluca Valentini, and Daniela Comelli. Combined photoluminescence and Raman microscopy for the identification of modern pigments: explanatory examples on cross-sections from Russian avant-garde paintings. *Heritage Science*, 7: 17, 2019. doi: 10.1186/s40494-019-0258-x.